HAL
open science

Accurate modelling of small-scale linear ion trap operating mode using He buffer gas to improve sensitivity and resolution for in-the-field mass spectrometry

Aurika Janulyte, Yves Zerega, Boris Brkić, Steve Taylor, Jacques Andre

To cite this version:

Aurika Janulyte, Yves Zerega, Boris Brkić, Steve Taylor, Jacques Andre. Accurate modelling of small-scale linear ion trap operating mode using He buffer gas to improve sensitivity and resolution for in-the-field mass spectrometry. Journal of Analytical Atomic Spectrometry, 2019, 10.1039/C9JA00017H . hal-02154778

HAL Id: hal-02154778

https://hal.science/hal-02154778v1

Submitted on 13 Jun 2019

HAL is a multi-disciplinary open access archive for the deposit and dissemination of scientific research documents, whether they are published or not. The documents may come from teaching and research institutions in France or abroad, or from public or private research centers.

L'archive ouverte pluridisciplinaire **HAL**, est destinée au dépôt et à la diffusion de documents scientifiques de niveau recherche, publiés ou non, émanant des établissements d'enseignement et de recherche français ou étrangers, des laboratoires publics ou privés.

Journal of Analytical Atomic Spectrometry

ARTICLE TYPE

Cite this: DOI: 10.1039/xxxxxxxxxx

Accurate modelling of small-scale linear ion trap operating mode using He buffer gas to improve sensitivity and resolution for in-the-field mass spectrometry

Aurika JANULYTE,[a] Yves ZEREGA,[b] Boris BRKIĆ,[c] Steve TAYLOR,[d] and Jacques ANDRE [b]

Received Date
Accepted Date

DOI: 10.1039/xxxxxxxxxx

www.rsc.org/journalname

Spectral peak separations of 4 m/z were previously measured using a small-scale mass spectrometer. In this paper the use of He buffer gas during mass analysis was investigated in order to obtain better peak separations (1 m/z) and to optimize the design prior to construction of a new linear ion trap (LIT) device with a novel electrode arrangement and operating mode. Ion/neutral collisions were simulated during LIT operation with an event driven statistical collision treatment tool using 3D electric field boundary element modelling software. Using He buffer gas during the LIT cooling step and assuming a collision-free isolation step during the LIT operating mode, 1 m/z separation can be obtained with also an increased instrument sensitivity. This requires adaptation of both the LIT operating mode and the LIT device configuration. These performance improvements come at the expense of an increase in the analysis duration time which however remains acceptable.

1 Introduction

Research work involving portable mass spectrometry for in-the-field application has accelerated since 2000[1]. Different types of radio frequency (RF) trapping analysers can be used within small instruments, and their miniaturisation has several advantages. For instance, with smaller internal radii, lower confinement voltages can be used at the same frequency[2]. However, a small containment volume can increase the space charge effect[3]. A linear ion trap (LIT) has a quadrupole field in the radial direction and a static field in the axial direction. Its geometrical shape leads to improved trapping efficiency upon ion injection along axial direction with large containment capacity with equivalent space charge, in comparison with a 3D trap[4].

The electronic control unit (ECU), which provides confinement and control voltages, requires functionality simplification for device portability. This can be achieved through the choice of the LIT operating mode. Only a single m/z ion is analysed with non-scanning mode[5] and using this mode, only the only DC potentials applied upon electrodes are switched for ion injection, isolation and ejection: the maximal amplitude of the isolation RF voltage is maintained constant during the sequence. The sequence can be reproduced with different maximal amplitudes of RF voltage to analyse a set of different m/z ions[6]. As a consequence, only DC potential changes are required with short rising/falling times at switching, without generating an RF voltage ramp. Operation in non-scanning mode has the advantages of faster operation (important for security applications in-the-field) and reduced false positives because possible interference compounds are screened out *a priori*.

In a portable instrument, air residue in the vacuum chamber is typically used as buffer gas as it may be easily introduced at gas/ion sampling. The collisions between confined ion and buffer gas result in a decrease of the ion kinetic energy with time.

With higher pressures (from 1 to 50 mtorr), ion neutral collisions reduce the stability region and the region in which mass-selective resonance ejection is performed. In addition, an increase of the pressure improves collision-induced dissociation efficiency and mass resolution[7].

The use of a buffer gas at lower pressures improves ion injection[8], resolution of mass-selective instability scan and ion isolation in 3D traps[9,10]. The effects of He buffer gas and ambient air have been characterised on the performance of a LIT with hyperbolic electrodes. An improvement of resolution and ion isolation was observed with He gas[11].

In an earlier paper, the authors reported the development of

[a] Aix Marseille Université, CNRS, PIIM - UMR7345, Centre de Saint Jérôme, 13397 Marseille Cedex 20 (13e arrdt), France. E-mail: aurika.janulyte@univ-amu.fr
[b] Aix Marseille Université, CNRS, MADIREL - UMR7246, Centre de Saint Jérôme, 13397 Marseille Cedex 20 (13e arrdt), France.
[c] BioSense Institute, University of Novi Sad, Dr Zorana Đinđića 1, 21 101 Novi Sad, Serbia.
[d] Department of Electrical Engineering and Electronics, University of Liverpool, Brownlow Hill, L69 3GJ, Liverpool, UK.

a portable device comprising a LIT operated in non-scanning mode[12]. An experimental mass separation of 4 u was obtained for methyl benzoate, 2-nitrotoluene and dimethyl methylphosphonate[13]. Since then the authors have shown the possibility of decreased mass separation (increased resolution) with spatial- and velocity-reduced ion distributions, when the LIT is operated close to the stability diagram apex[14]. The conclusions of these studies led the authors to simulate the use of He buffer gas cooling in order to obtain a mass separation of 1 u. Prior to design and realisation of this new LIT device with an electrode arrangement allowing He entrance and fast pumping, they decided to simulate the effects of collisional cooling at each stage of a non-scanning LIT with hyperbolic electrodes. Although He buffer gas use could be disadvantageous for device portability, it was chosen instead of residual ambient air because of the improved performance that may be obtained. Many recent simulation papers neglect the influence of the RF trapping field by using the pseudo-potential approximation and consider that collisions induce a damping effect upon ion trajectories[15,16]. However, Schwarz emphasised in 2008 the necessity for a microscopic description of the RF heating and to take into account the statistical nature of the collisions[17]. If this is not done, the effectiveness of the cooling process can be significantly overestimated. The best visual evidence is given in Fig. 3 of Ref.[17], where the radial position as a function of axial position of an ion is compared for a viscous damping approach and a microscopic description of collisions.

The simulation in this uses a realistic electrode design and an accurate Boundary Element Method (BEM) to calculate the electric field for computation of the individual ion trajectories using the Charged Particle Optics (CPO) software[18]. A collisional computation tool has been developed and added to CPO which allows LIT pressure dependence to be modelled which is essential for accurate simulation. The recommendations of Schwarz have been taken into account in our simulations at the expense of the computational time duration. Since an accurate characterisation of collisional effects is required for each time step of the non-scanning mode sequence, the instants of collision are computed by an event-driven m using randomised probability computation methodology. The ion-buffer gas interaction is simulated by a hard-sphere model leading to a modification of the ion velocities when collision occurs.

The aim of this simulation study is therefore the accurate modelling of the LIT configuration in non-scanning mode with collisional cooling to obtain a mass peak separation equal to 1 m/z with a greater sensitivity thanks to an increase of the number of ions.

2 Materials and methods

2.1 LIT design and operating conditions

The design of the LIT modelled in this study is schematically represented in Figure 1. It is composed of four hyperbolic electrodes whose ends are closed by two flat disks (lenses). The physical centre of the LIT is the origin of the coordinate system. The hyperbolic electrodes are truncated at $3r_0$. The smallest distance separating a hyperbolic electrode from the Oz axis is $r_0 = 2$ mm. The length of the hyperbolic electrodes is $2z_0 = 40$ mm. An electron impact ion source and a set of extracting, focusing and grounded lenses are coupled to the LIT. The ions are injected with 3 eV energy. For more details on ion injection simulation with experimental results, see references[12,14].

The non-scanning mode consists in a series of m/z mass analysis sequences[12,13]. Each sequence comprises four steps: injection, cooling, isolation and total ejection.

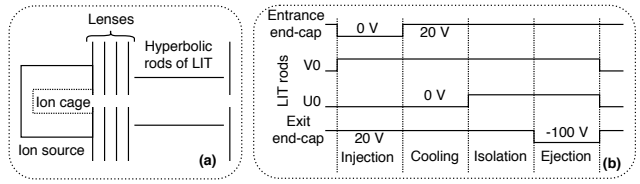

Fig. 1 (a) LIT and open EI ion source coupling. (b) Applied potentials according to the steps (injection, cooling, isolation and total ejection) of a sequence for m/z ion mass analysis.

Figure 1 describes the potentials applied to the electrode for each step of the sequence. A symmetrical configuration is applied to the hyperbolic electrodes of the trap: $V(t) = U_0 + V_0 \cos(\Omega t + \varphi)$ on the pair of x-axial electrodes and $-V(t)$ on the pair of y-axial electrodes. The frequency is $\Omega/(2\pi) = 1$ MHz. The maximal amplitude of the RF confinement voltages is maintained at a constant value during the steps of the sequence. Only the DC voltages applied to hyperbolic and end-cap electrodes are modified in order to: enter the ions, and then eject them from the trap; operate the LIT in RF only mode for ion injection and cooling; and operate the LIT close to the apex for ion isolation. This simplifies the conception of the voltage generating device (ECU) and guarantees a better stability of the voltages needed for ion confinement. During the injection step, 0 V is applied to the input disk of the trap, 20 V is applied to the output disk, and $U_0 = 0$ V and $V_0 = V_{apex}$ of the m/z ion being analysed. During the cooling step, the trap operates in RF only mode with both end-caps biased at 20 V. During the isolation step, the DC confinement voltage is instantaneously switched from $U_0 = 0$ to U_{apex}. Finally, during the ejection step, the voltage applied to the output disk is switched to -100 V to extract the ions out of the trap and propel them towards the detector.

2.2 Ion/neutral collision modelling and computational tool

The ion/neutral interaction is assumed to be elastic and simulated by means of a hard-sphere model. With respect to this model, the ion and neutral velocities are modified by collision. In the centre-of-mass system, the total kinetic energy is conserved and scattering is isotropic.

For determination of instants of collision, an event-driven approach results in a more accurate and efficient simulation than a time-driven one.

Ion trajectories are computed using the CPO software[18] with a small constant step time $\Delta t = 5 \times 10^{-5}$ ms. At the end of each step time, an in-house subroutine is called for ion-neutral collision treatment.

This journal is © The Royal Society of Chemistry [year]

The main event-driven simulation loop works as follows:

At each step time of ion trajectory computation, an elementary probability, denoted as p_{ce}, is computed from the following equation:

$$p_{ce} = \rho_G \sigma_{IG} \| \vec{v_I} - \vec{v_G} \| \Delta t \quad (1)$$

with ρ_G (atoms/m^3) the He buffer gas density; $\sigma_{IG} = 3.5 \times 10^{-19}$ (m^2) an estimation of the total scattering cross-section between m/z 100 ion and He atom (see Page 20 of Reference[19]); $\vec{v_I}$ the ion velocities computed by CPO; and $\vec{v_G}$ the He buffer gas velocities.

The He buffer gas velocities are drawn from three zero-centred Gaussian density functions with standard deviations $\sigma_{Gx} = \sigma_{Gy} = \sigma_{Gz} = \sqrt{k_B T / m_G}$, with $k_B = 1.38 \times 10^{-23}$ J×K^{-1}, the Boltzmann constant and T the buffer gas temperature (K).

At each step time, the elementary probability p_{ce} is summed with the previously computed ones. This summation improves the estimation of each elementary probability computed from a single sample.

When the sum, denoted as p_c, exceeds $\varepsilon = 10^{-2}$, a value is drawn from a uniform distribution on $[0,1]$, and if this value is lower than p_c then a collision occurs. The value $\varepsilon = 10^{-2}$ is the best compromise between precision and fast computation ensuring that no more than one collision occurs and that positions and velocities of ions are almost constant.

When a collision occurs, the final ion velocities are modified. In the centre-of-mass system, the velocity of the ion after the collision is expressed in accordance with energy and momentum conservation:

$$\vec{v}'_{IB} = \frac{m_G}{m_G + m_I} \| \vec{v}_I - \vec{v}_G \| \vec{n} \quad (2)$$

with m_G (kg) and m_I (kg) the masses of He buffer gas and ion, respectively; and $\vec{n}$ a unitary vector defining the ion direction after collision.

Hard sphere scattering is isotropic in the centre-of-mass and does not depend on incident ion direction. The two scattering angles θ and φ (using spherical coordinates) are drawn from $\theta = \arccos(1 - 2u_1)$ and $\varphi = 2\pi u_2$, respectively, with u_1 and u_2 two uniform distributions on $[0,1]$.

Then, the new ion velocity is calculated in the coordinate system from equation:

$$\vec{v}'_I = \frac{m_G}{m_G + m_I} \| \vec{v}_I - \vec{v}_G \| \vec{n} + \frac{m_G \vec{v}_G + m_I \vec{v}_I}{m_G + m_I} \quad (3)$$

After collision treatment, the sum p_c is reset to zero.

The trajectory computation stops when the confinement time exceeds a fixed value.

2.3 Testing the validity of the computational tool

For testing, the operating conditions are: number of ions = 200; m/z = 100; $V_0 = 28.9$ V; $U_0 = 0$ V.

As expected, the number of collisions is proportional to the pressure (Table 1). The mean value of p_c is slightly higher than $\varepsilon = 10^{-2}$ and increases with pressure. The number of values involved in computation of $\overline{p}_c$ decreases when pressure increases. By this means the model could produce results corresponding to higher values of He gas temperature or density (pressure) than the input values. The highest pressure value used in simulation, *i.e.* $p_G = 1 \times 10^{-3}$ torr, gives $\overline{p}_c \approx 1.0517 \times 10^{-2}$ with $\sigma_{p_c} = 0.0388 \times 10^{-2}$. It is the maximal value of the buffer gas pressure that can be used within this model, with the time step duration $\Delta t = 5 \times 10^{-5}$ ms for ion trajectory computation.

Table 1 Number of collisions, mean value and standard deviation of p_c.

p_G (torr)	Number of collisions	$\overline{p}_c$ (10^{-2})	σ_{p_c} (10^{-2})
1×10^{-3}	21 055	1.0517	0.0388
5×10^{-4}	10 592	1.0279	0.0209
3×10^{-4}	6 981	1.0175	0.0129
1×10^{-4}	2 178	1.0068	0.0047

The set of times at which collision occurs is recorded. The set of time intervals between two collisions (denoted as τ_c) can be then computed. The number of collision occurrences versus time interval between two collisions is then computed by time intervals of 20 μs (Figure 2). Assuming that the number of collision occurrences can be interpolated by an exponentially decreasing function for values greater than zero: $\exp(-x/\overline{\tau}_c)$ with $\overline{\tau}_c$ the mean value. From results of Figure 2, it is found that $\overline{\tau}_c$ is inversely proportional to the buffer gas pressure. The variable τ_c can be then used as a criterion for studying the time to reach the ion equilibrium state.

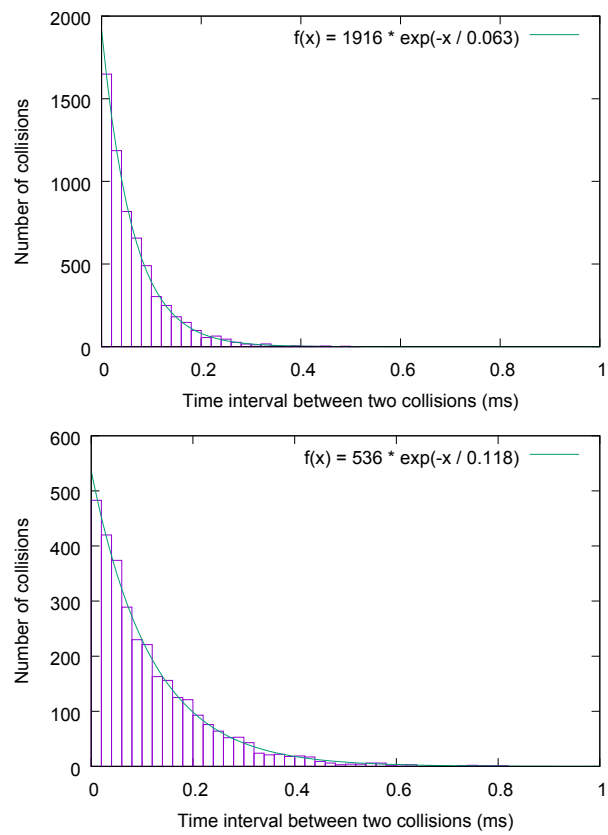

Fig. 2 Number of collisions versus time intervals between two collisions for $p_G = 1 \times 10^{-3}$ (top) et 5×10^{-4} torr (bottom).

3 Results

3.1 Injection step

For ion injection, the trap is operated in RF only mode with $U_0 = 0$ V and $V_0 = 28.9$ V for m/z 100 ions. We have previously estimated that the trap filling time (or maximal residence time of ions in the trap) from a short-time pulse ion injection is almost 150 μs for m/z 100 ions[14]. Additional computations have been performed with the same design and operating conditions except that simulation tool involves collisional processing.

Results are given in Figure 3 for RF confinement potential phase $\varphi = 0$ and three values of the buffer gas pressure.

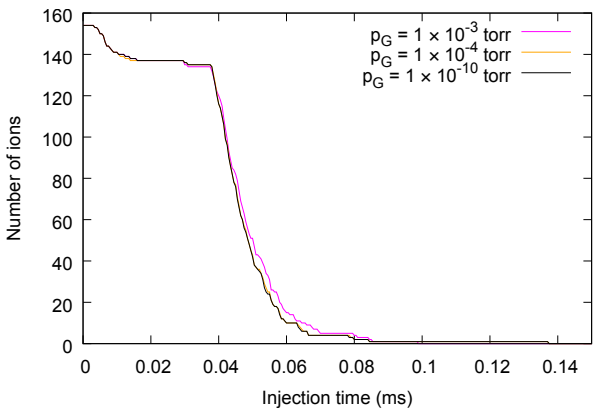

Fig. 3 Number of injected m/z 100 ions versus injection time for $p_G = 1 \times 10^{-3}$, 1×10^{-4} and 1×10^{-10} torr.

Only a small increase of the number of ions is observed for the highest pressure $p_G = 1 \times 10^{-3}$ from the injection time 40 μs. The ions undergo an average of 2 collisions during injection. The maximal number of collisions, *i.e.* 9 collisions, has been observed for two ions having the highest residence times and a complete path in the LIT.

As demonstrated in the next section, we can assume that the position and velocity distributions of ions at steady-state are not modified by collisional processes due to the small number of collisions.

3.2 Cooling step

For ion cooling, the trap is operated in RF only mode with $U_0 = 0$ V, and $V_0 = V_{apex} = 28.9$ V for m/z 100 ions and $V_0 = V_{apex} = 86.7$ V for m/z 300 ions. The initial ion distributions of cooling step are the ion distributions at the end of collision-free injection[14]. The main objective is to determine the influence of the collisions on the number of confined ions and on the evolution of position and velocity ion states, and the minimum time of the ion cooling step, time from which we can consider that the ion cloud has reached the equilibrium state.

3.2.1 Number of confined ions

From trajectories computed by CPO, the number of ions can be computed for different confinement times. The relative number of confined ions of m/z 100 is plotted versus cooling time in Figure 4.

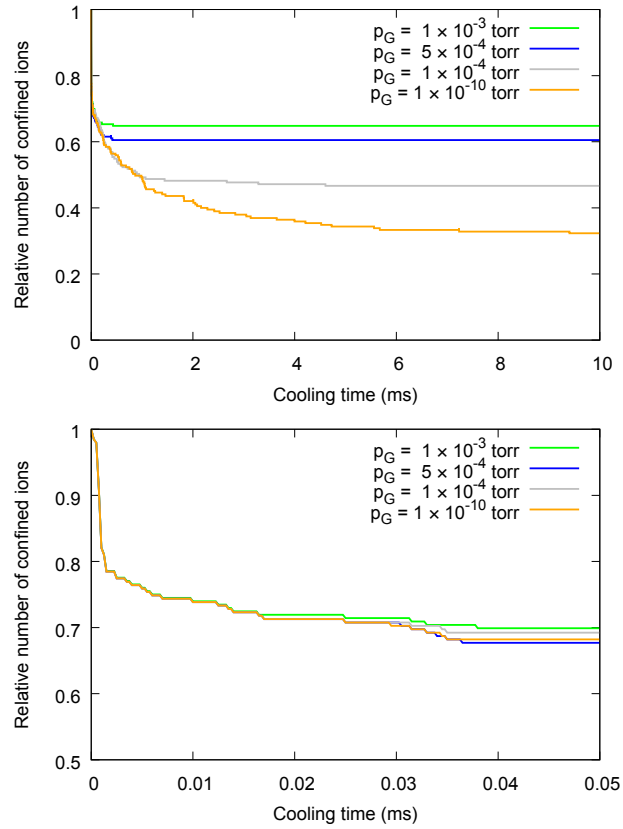

Fig. 4 (Top curve) Relative number of m/z 100 confined ions versus confinement/cooling time for different He buffer gas pressures: $p_G = 1 \times 10^{-3}$, 5×10^{-4}, 1×10^{-4} and 1×10^{-10} torr. (Bottom curve) enlarged view for the lowest confinement times.

A first ion loss (the decrease from 1 to 0.8) is observed for the first confinement times, corresponding to a micro period of the confinement field (1 μs). One can assume that these lost ions have initial conditions that fall outside the phase-space acceptance ellipses in the radial directions. Then, a progressive loss of ions occurs due to non-linearities.

Between 15 and 20 μs the curves have different behaviours: an ion loss is observed for the lowest pressures while not for $p_G = 1 \times 10^{-3}$ torr. One can assume that a collision has occurred leading to stabilisation of the ion trajectory for $p_G = 1 \times 10^{-3}$ torr. Over a time interval of 10 ms, more ions remain trapped with collisions: the higher the pressure, the greater the number of confined ions. For a cooling time of 4.5 ms, the number of confined ions increases with He buffer gas pressure, until about 0.66 for $p_G = 1 \times 10^{-3}$ torr.

In Figure 5, the relative number of confined ions of m/z 100 is plotted versus He buffer gas pressure at cooling time 4.5 ms. The number of confined ions starts to increase from $p_G = 1 \times 10^{-5}$ torr, then tends to stabilise to 0.66 from $p_G = 1 \times 10^{-3}$ torr. The same shape of variation in the number of ions has been observed in experiments, for instance, to fill up a 3D Paul trap of 1 cm^3 volume when ions are injected along the axial direction (see Figure 17 in Page 52 of Reference[20]) and to accumulate ions in a linear radiofrequency trap of the ISOLTRAP mass spectrometer (see

This journal is © The Royal Society of Chemistry [year]

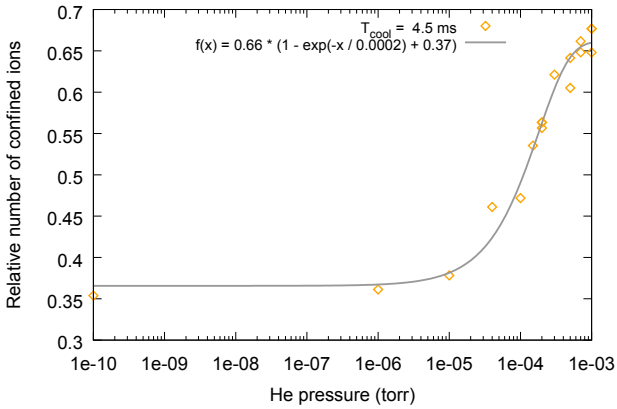

Fig. 5 Relative number of m/z 100 confined ions versus He buffer gas pressure for cooling time equal to 4.5 ms.

Figure 20 in Page 27 of Reference[21]).

3.2.2 Equilibrium state and cooling time

For each ion, the pair "time interval between two collisions" and "confinement time" or "instant of collision", denoted as (τ_c, t_c) has been recorded when collision occurs. The mean value $\overline{\tau}_c(t_i)$ is calculated from pairs such as the value of $t_c \in [t_i - T_e/2, t_i + T_e/2]$, with $t_i = iT_e$, and $T_e = 90$ μs for m/z 100 ions and 180 μs for m/z 300 ions. $\overline{\tau}_c(t_i)$ is plotted in Figure 6 for $p_G = 1 \times 10^{-3}$ torr.

The central limit theorem establishes that the values of $\tau_{sc}(t_i)$ are normally distributed around the mean value $\overline{\tau}_c(t_i)$ with standard deviation : $\sqrt{E\left[(\tau_c(t_i) - \overline{\tau}_c(t_i))^2\right]/N_{col}(t_i)}$, where $N_{col}(t_i)$ is the number of collisions in time interval $[t_i - T_e/2, t_i + T_e/2]$. In Figure 6, the error bars represent the two standard deviation limits around the mean.

The computed values are interpolated by the curve $\overline{\tau}_c(t_i) = (\overline{\tau}_c(\infty) - \overline{\tau}_c(0))(1 - \exp(-t_i/\tau_r)) + \overline{\tau}_c(0)$ (curve of Figure 6). The mean value of the time interval between two collisions tends to the constant value $\overline{\tau}_c(\infty) = 0.067$ ms for m/z 100 ions, with the relaxation time $\tau_r = 1.5$ ms. The parameters of the interpolation curve are valid as these curve falls within the error bars.

One can assume that the equilibrium state is reached when the criterion $\tau_c(t_i)$ does not evolve. The equilibrium time or cooling time is expressed as: $\tau_{eq} = 3\tau_r = 4.5$ ms for m/z 100 ions. The number of collisions necessary to cool the ion cloud is calculated by: $N_{col,eq} = \tau_{eq}/\overline{\tau}_c(\infty) \simeq 70$ collisions.

As a result, the time duration of the cooling step is $T_{cool} = 4.5$ ms for m/z 100 ions and 14 ms for m/z 300 ions with $p_G = 1 \times 10^{-3}$ torr. For lower values of the buffer gas pressure over few orders of magnitude, the cooling time can be estimated being linearly related in inverse proportion to the buffer gas pressure.

3.2.3 Position and velocity distributions of the ion cloud

The position and velocity distributions at the end of injection step and at the end of cooling step are compared for m/z 100 ions in Figure 7. The duration of the cooling stage is 4.5 ms with $p_G = 1 \times 10^{-3}$ torr. The final time of cooling step corresponds to the phase zero of the RF confinement field.

When they are injected the ions enter the LIT at different RF

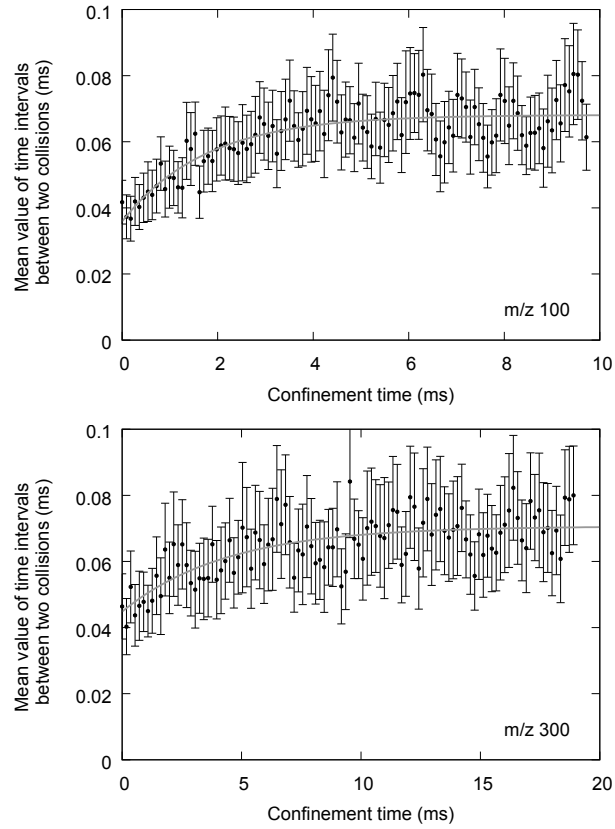

Fig. 6 Mean values of time intervals between two collisions versus confinement time with $p_G = 1 \times 10^{-3}$ torr. (Top curve) m/z 100 ions. (Bottom curve) m/z 300 ions.

phases of the confinement field. As a consequence, the radial distributions in position and velocity are identical and differ from Gaussian in that the distributions have a heavier tail than a Gaussian distribution. The axial-position distribution is quasi-uniform due to the U-shaped potential well along the axial direction. The axial-velocity distribution shows two classes of velocities corresponding to the outward and return paths of the ions in the trap. Using equation $(1/2)m(\Delta v)^2 = q(\Delta V)$ (difference of kinetic and potential energy between source and trap centre) and assuming that initial velocity of neutral in the ion source is negligible, with ion source biased at 3 V and trap centre at 0 V, the estimated value of maximal axial velocity in the trap is 2500 m/s for m/z 100 ions and 1400 m/s for m/z 300 ions.

When the ion cloud is cooled at equilibrium state (at 4.5 ms with $p_G = 1 \times 10^{-3}$ torr) the radial distributions tend to Gaussian functions with different standard deviations between to x- and y-direction, and between position and velocity. The ion cloud is cooled and the ions oscillate synchronously according to RF confinement field. The ions remain quasi-uniformly distributed in the axial direction with lower trajectory extensions. The axial velocity distribution tends to a Gaussian function.

3.2.4 Standard deviation of ion velocities and mean kinetic energy

The standard deviation of ion velocities and mean ion kinetic energy versus confinement/cooling time are plotted in (Figure 8)

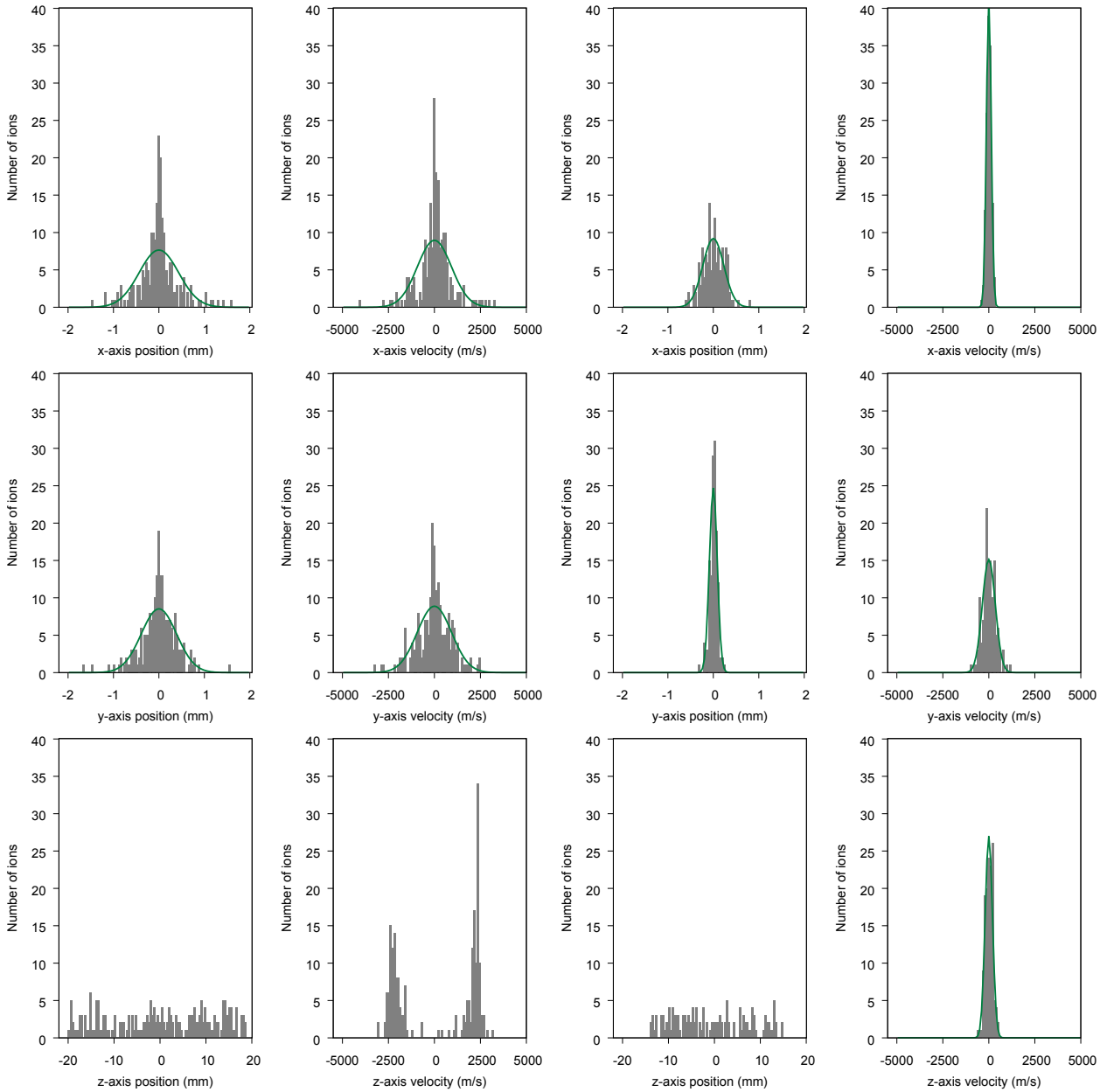

Fig. 7 (column 1) Distributions of x-, y- and z-axis positions at the end of injection step; (column 2) Distributions of x-, y- and z-axis velocities at the end of injection step; (column 3) Distributions of x-, y- and z-axis positions at the end of the cooling step; (column 4) Distributions of x-, y- and z-axis velocities at the end of the cooling step. m/z 100 ions. The duration of the cooling step is 4.5 ms with $p_G = 1 \times 10^{-3}$ torr. The green curves are the Gaussian functions computed from the values of ion positions and velocities.

This journal is © The Royal Society of Chemistry [year]

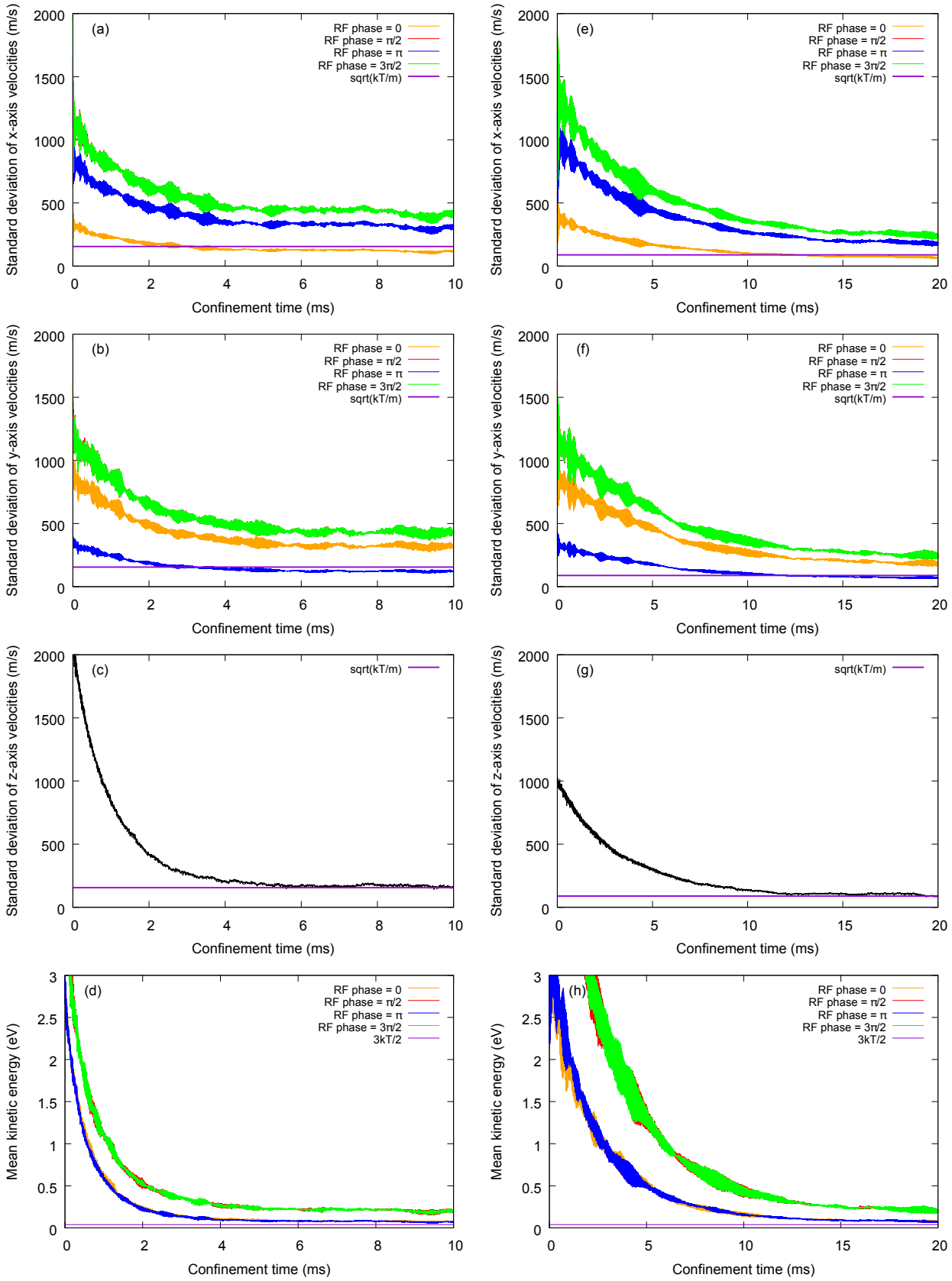

Fig. 8 Standard deviation of ion velocity in (a) (e): x-direction, (b) (f): y-direction, (c) (g): z-direction and (d) (h) mean value of ion kinetic energy for $p_G = 1 \times 10^{-3}$ torr. Curves (a), (b), (c) and (d) m/z 100 ions. Curves (e), (f), (g) and (h) m/z 300 ions. For ion kinetic energy and for standard deviations of ion velocity in x- and y-directions, four curves are plotted for 0, $\pi/2$, π and $3\pi/2$ phases of the RF confinement field.

for $p_G = 1 \times 10^{-3}$ torr. For ion kinetic energy and for standard deviations of ion velocity in x- and y-directions, four curves are plotted for 0, $\pi/2$, π and $3\pi/2$ phases of the RF confinement field. For each phase, the points are separated by 1 μs.

The standard deviation of ion velocities and mean value of ion kinetic energy decrease with time. These values tend to a constant value from about 4.5 ms confinement time for m/z 100 ions and about 14 ms for m/z 300 ions. This confirms the previous estimation of the cooling time for $p_G = 1 \times 10^{-3}$ torr.

The minimal values of the standard deviation of x-direction are obtained for 0 phase. At equilibrium, the value is lower than $\sqrt{k_B T/m_I}$ = 155 m/s for m/z 100 ions and 89 m/s for m/z 300 ions.

The mean value of kinetic energy is maximal for $\pi/2$ and $3\pi/2$ phases and minimal for 0 and π phases. At equilibrium, the kinetic energy remains slightly higher than $3k_B T/2$ = 0.0388 eV as the ions experience RF field (RF heating).

3.3 Isolation step

The isolation step allows us to trap ions of given m/z. In this simulation work, it is assumed that U_0 is instantaneously switched from zero to U_{apex}, a value close to the apex of the stability diagram. The stability diagram is that of a m/z 100 ion (or m/z 300 ion) crossing through an "equivalent" quadrupole mass filter (the term is defined just below). In order to have a finer characterisation of the step, the spectral response has been calculated for the scan line giving a mass separation of 1 m/z. The influence of the number of ions involved and step duration has been studied for mass separation of 1 m/z.

3.3.1 Stability diagram close to apex

The theoretical stability diagram of an "equivalent" Quadrupole Mass Filter (QMF) has been compared to the stability diagram of the LIT.

The equivalent QMF is a mass filter having hyperbolic electrodes located at a same distance (*i.e.* $r_0 = 2$ mm) than the LIT and having an infinite length. The boundaries of the theoretical stability diagrams for m/z 99, 100 and 101 ions have been computed by means of the matrix method[22] and plotted in Figure 9. For the QMF, the scan line $U_0 = 0.17 \times V_0 - 0.096$ provides mass separation of 1 m/z (Figure 9).

To delimit the boundaries of the LIT stability diagram, the numbers of m/z 99 and m/z 100 ions have been computed from CPO trajectories for a great number of operating points in the plane (U_0, V_0) close to the apex (Figure 9). As it is very time consuming, the contour lines of only two different m/z values have been calculated and plotted for LIT, while the theoretical stability diagrams of three different m/z values have been plotted in order to show the scanline providing separation of 1 m/z. The initial conditions of ion cloud are the final conditions of the cooling stage with $p_G = 1 \times 10^{-3}$ torr. The ions are confined collision-free for 100 μs.

A shift has been observed between QMF and LIT diagrams. In Figure 9, the contour lines have been shifted according to the following relations: $U_0^{\mathrm{QMF}} = U_0^{\mathrm{LIT,CPO}} - 0.01$ V and $V_0^{\mathrm{QMF}} = V_0^{\mathrm{LIT,CPO}} - 0.06$ V in order to locate inside the theoretical stability diagrams.

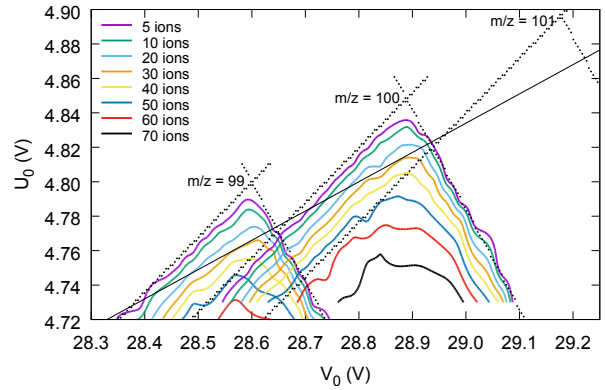

Fig. 9 Number of ions in the plane (U_0, V_0) for m/z 99 and m/z 100 ions. The black dots represent the boundaries of the stability diagrams of the equivalent QMF for m/z 99, m/z 100 and m/z 101 ions. The contour lines represent the number of confined ions in the LIT; they have been computed only for m/z 99 and m/z 100 ions as computation is very time consuming. The straight line is the scan line $U_0 = 0.17 \times V_0 - 0.096$ providing separation of 1 m/z.

The static electric field introduces a defocusing effect in both radial directions leading to a stability diagram different from that of the equivalent QMF[23,24]. By limiting the development of the potential to the quadruple term, the apex of the LIT can be shifted to a higher value of V_0 and to a lower of U_0. This is therefore not compatible with the observed shift that comes from electrode segmentation in CPO. The potential is applied at the centre of the segment. Due to the convex shape of the electrodes inside the LIT, the electric potential is applied at a distance larger than that expected. The upper potential correction must be applied and is taken into account in the entire simulation process.

3.3.2 Minimal length of equivalent QMF

It is interesting to estimate the minimal length of the equivalent QMF using the same initial conditions than the LIT.

For m/z 100 ions, the trajectories in the equivalent QMF have been computed by solving 2D Mathieu equations using an RK4 method with 400 points per period of the confinement field. Ion confinement is He-free here. The initial conditions are those at the end of cooling at T_{cool} = 4.5 ms, except for the following modifications: the axial positions are set to 0 mm and the axial velocities are centred on the equivalent velocity corresponding to a kinetic energy of 3 eV (the potential energy difference between ion source and the centre of the LIT).

The number of confined ions has been computed from trajectories for several operating points located on the scan line to obtain the mass spectrum of m/z 100 ions at different mean values of time-of-flight (curve (d) of Figure 13). Separation of 1 m/z is obtained for a mean value of time-of-flight greater or equal to 200 μs.

The optimal operating point $U_0 = 4.817$ V and $V_0 = 28.9$ V is chosen on the scan line inside the stability diagram of m/z 100 ion. The evolution of axial position distribution of m/z 100 ions according to the time-of-flight in the equivalent QMF is given in

This journal is © The Royal Society of Chemistry [year]

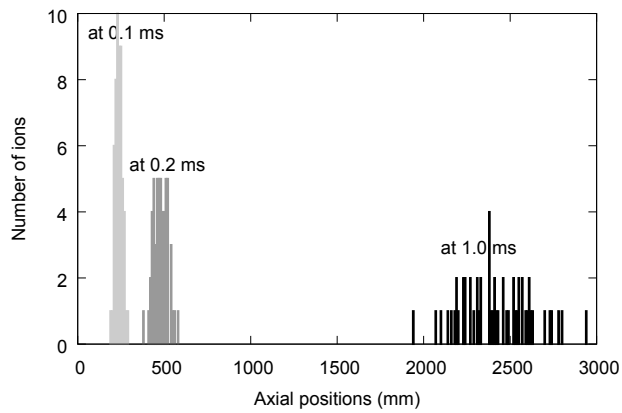

Fig. 10 Axial position distributions of m/z 100 ions in the equivalent QMF at $U_0 = 4.817$ V and $V_0 = 28.9$ V for three values of the transfer time.

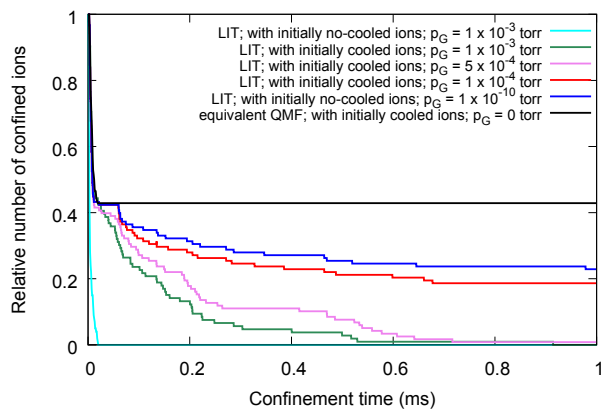

Fig. 11 Number of confined ions during isolation step at $U_0 = 4.817$ V and $V_0 = 28.9$ V for m/z 100 ions.

Figure 10. To obtain a separation of 1 m/z for a time-of-flight greater or equal to 200 μs, the equivalent QMF must be at least 500 mm long, while LIT length is 40 mm and this comparison demonstrates the advantages of the LIT in comparison to a QMF.

3.3.3 Number of ions at the optimal operating point

The optimal operating point at $U_0 = 4.817$ V and $V_0 = 28.9$ V was chosen on the scan line for the stability diagram of m/z 100 ion. The number of ions has been computed versus confinement time for the equivalent QMF and for the LIT with initially cooled or no-cooled ions (during the cooling step) and different He gas pressures during the isolation step (Figure 11).

Without a cooling prior to the isolation step, when collisions occur (with $p_G = 1 \times 10^{-3}$ torr), the ions are instantaneously lost. With a cooling step, the lower the He pressure, the greater the number of confined ions. Even without cooling prior to the isolation step, the greatest number of confined ions is obtained collision-free during isolation step (with $p_G = 1 \times 10^{-10}$ torr).

In Figure 12, the locations in the y- and z-directions of ions lost in the x-direction are plotted versus confinement time for $p_G = 1 \times 10^{-10}$ and 1×10^{-3} torr. During collision-free trapping, the ions are preferentially lost in the y-direction, due to phase of the RF confinement field. During the initial instants of confinement,

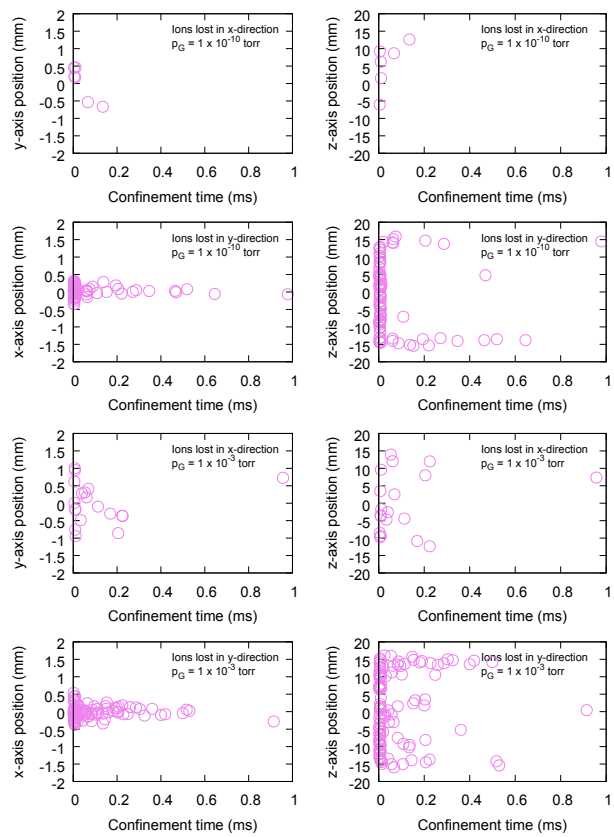

Fig. 12 Radial and axial positions of ion lost in x- and y-directions versus confinement time for m/z 100 ions, $p_G = 1 \times 10^{-10}$ and 1×10^{-3} torr.

the ion loss is not linked to the axial ion position. The lost ions have stable radial trajectories but with large excursions resulting in collision with trap electrodes, mainly in the y-direction and this is because the trap operating point is close to iso-beta line $\beta_y = 1$. For larger confinement times, ion loss occurs when the ions are axially located at both ends of the trap, where non-linearities exist. This mode of ion loss is due to energy exchanges from the axial to the radial direction.

With collisions ($p_G = 1 \times 10^{-3}$ torr), additional ion losses occur in both radial directions, even when ions do not experience non-linearities.

3.3.4 Spectrum of m/z 100 ions

To establish the spectrum of m/z 100 ions, the trajectories of 100 ions have been computed for the maximal confinement time of 500 μs. The spectrum comes from a series of non-scanning mode sequences with the same cooled-ion cloud as the initial condition, and with different operating points belonging to the scan line providing mass separation of 1 m/z. As a consequence, it is not a spectrum measured by moving the operating point along the scan line. In the cooling step, the necessity of ion cooling to greatly increase the number of ions has been shown. So, only a cooled-ion cloud has been considered here.

In Figure 13, spectra have been plotted for different isolation step durations and He gas pressures during the isolation step. Contrary to quadrupole mass filter (curve (d)), the maximal number of ions decreases with time in the collision-free case with He pressure equal to $p_G = 1 \times 10^{-10}$ torr (curve (a)). This ion loss is due to non-linearities: there are a large number of resonance lines close to the stability diagram apex[23]. This ion loss increases when He gas pressure increases (curves (b) and (c)). Consequently, collisions induce additional ion losses when the trap is operated close to apex of the stability diagram.

3.3.5 Spectrum of m/z 300 ions

To achieve 1 m/z mass separation in the equivalent QMF with m/z 300 ions, the scan line used is: $U_0 = 0.17 \times V_0 - 0.225$. Spectra have been calculated for different durations of isolation step in the collision-free case (with $p_G = 1 \times 10^{-10}$ torr) with cooled initial ion distributions (cooling step at $p_G = 1 \times 10^{-3}$ torr) (Figure 14). The relative number of ions is almost the same than with m/z 100 ions. Mass separation is 1 m/z.

For m/z 100 and 300 ions, with collision-free confinement in the LIT, mass separation of 1 m/z is achieved for an isolation step duration of about 200 μs with a relative number of ions of 30 % at peak maximum. So, it is important to adapt the operating mode to increase the number of ions.

4 Discussion and conclusions

The performance comparison, *i.e.* sequence duration and number of ions, for m/z 100 ions and mass separation of 1 m/z is given in Table 2 according to He pressure and non-scanning mode sequence, either with constant He pressure, or with an additional He removal step. The relative number of ions is calculated by dividing the number of ions measured with a LIT by the number of ions measured with an equivalent QMF of infinite length. The number of ions measured with the equivalent QMF is the number of ions present in the QMF after time duration T_{isol}, here in Table 2 equal to 0.2 ms, as required mass separation is 1 m/z.

Table 2 Comparison of LIT performances (*i.e.* sequence duration and number of ions) for m/z 100 ions according to non-scanning mode sequence either with constant He pressure, or with an additional He removal step. (*) estimated value deduced from simulation. (**) estimated value according to[11,25].

Sequence type	p_G (torr)	Duration (ms)	Number of ions (relative LIT/QMF)
Cooling step	1×10^{-3}	4.5	$68/77 \equiv 88\%$
Isolation step	1×10^{-3}	0.2	$15/45 \equiv 33\%$
Sequence total		~5.0	29%
Cooling step	5×10^{-4}	9.0	$61/77 \equiv 79\%$
Isolation step	5×10^{-4}	0.2	$25/45 \equiv 55\%$
Sequence total		~9.5	43%
Cooling step	1×10^{-4}	45 (*)	$45/77 \equiv 58\%$
Isolation step	1×10^{-4}	0.2	$30/45 \equiv 67\%$ (*)
Sequence total		~45.5	39%
Cooling step	1×10^{-3}	4.5	$68/77 \equiv 88\%$
He removal step		1000 (**)	100% (*)
Isolation step	free-He	0.2	$33/45 \equiv 73\%$
Sequence total		~1005	64%

The first three horizontal blocks of the table concern the non-scanning mode sequence with constant He pressure for three different values of He pressure. For $p_G = 1 \times 10^{-4}$ torr, the cooling step duration has been estimated at 45 ms, if we assume that the cooling duration is inversely proportional to He pressure. For the isolation step, the number of ions has been estimated between those obtained with $p_G = 5 \times 10^{-4}$ torr and He-free. There exists an optimal value of the number of ions of about 43% remaining at the end of the isolation step with this operating mode for $p_G = 5 \times 10^{-4}$ torr. In that case the sequence duration is less than 10 ms.

The last horizontal block concerns the non-scanning mode sequence with an additional He removal step. The He gas in this case may be introduced by means of a pulse valve. A He removal step is added prior to isolation step with He valve closed, in order to operate He-free the LIT at apex during isolation step[11]. Its duration has been estimated at 1 s according to work described in[25]. With this operating mode, the number of ions remaining at apex is increased to a value of about 64% at the expense of the sequence duration estimated to a few seconds. For m/z 300 ions, a same number of ions is obtained, however the cooling time is 14 ms.

In order to reduce analysis time duration, two LIT devices could be used: the first one operated in the cooling mode with He buffer gas and the second one operated He-free for mass isolation providing that the maximum number of ions can be transferred between the two devices and the ion states in the radial directions are not modified.

In order to increase mass separation, the operating point of the isolation step can be chosen closer to the stability diagram apex, however the initial number of ions will be lower. For instance, deduced from Figure 9, the relative number of ions is 30 % for mass separation of 1 m/z, and less than 10 % for 0.5 m/z.

Furthermore, both the sensitivity and mass separation could

This journal is © The Royal Society of Chemistry [year]

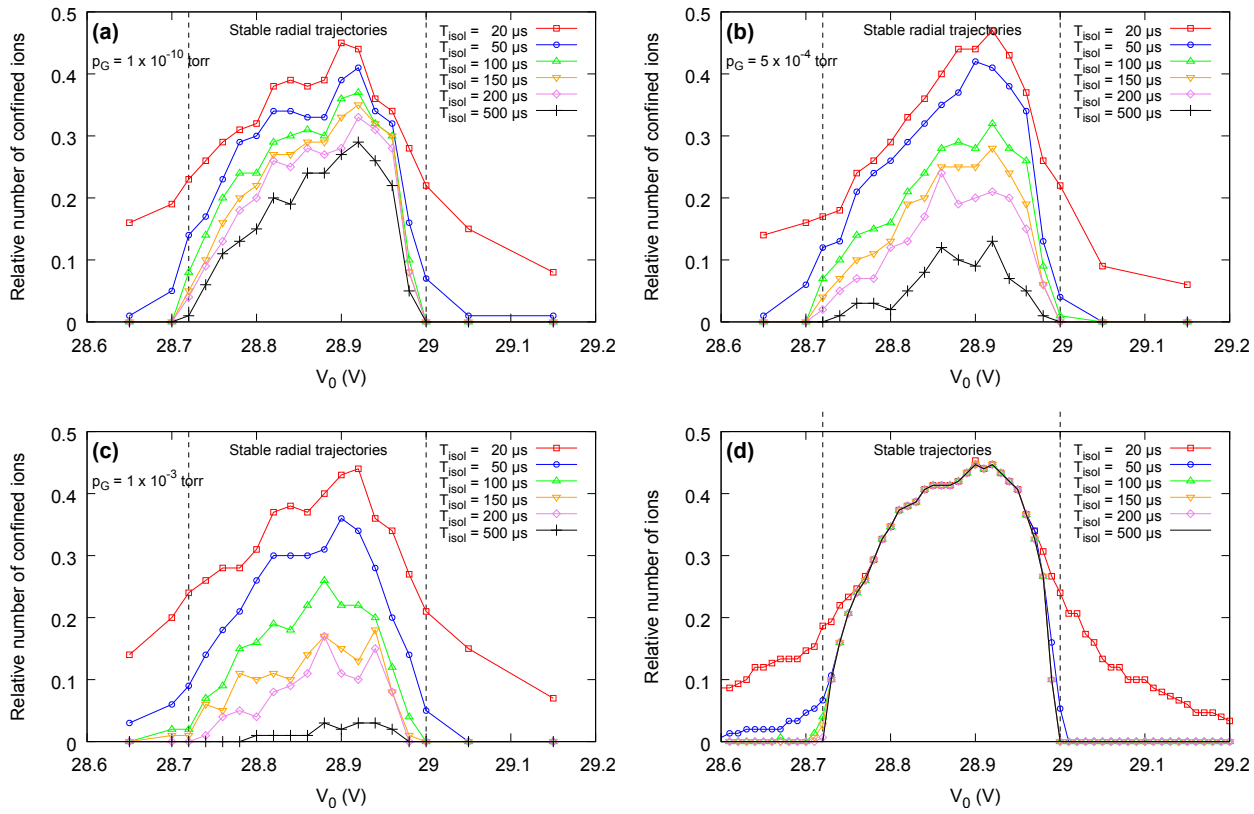

Fig. 13 Mass peaks of m/z 100 ions confined in the LIT for different isolation step durations T_{isol} and different He gas pressures $p_G = 1 \times 10^{-10}$ (a), 5×10^{-4} (b) and 1×10^{-3} torr (c). Mass peak of m/z 100 ions passing through equivalent quadrupole mass filter without collisions (d).

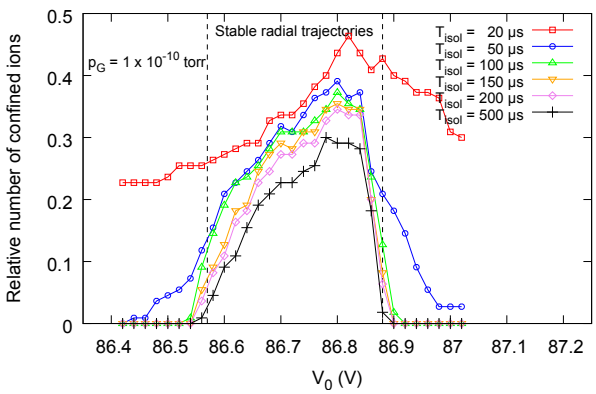

Fig. 14 Mass peaks of m/z 300 ions confined in the LIT for different durations T_{isol} of isolation step and with He gas pressure $p_G = 1 \times 10^{-10}$ torr.

be increased by using a specific potential ramp to move the LIT operating point in the stability diagram from the centre (RF only mode for cooling step) toward apex (for isolation step).

These promising results indicate the feasibility of this non-scanning technique for portable in-the-field mass spectrometer. Applications include detection of drugs of abuse, explosives and other security threats as well as point-of-use biomedical analyses for healthcare diagnostics.

Conflicts of interest

There are no conflicts to declare.

Acknowledgements

The authors would like to acknowledge funding provided from the European Commission under its FP7 programme, grant agreement no 285045 (SNIFFLES).

Notes and references

1 S. A. Smith, C. C. Mulligan, Q. Song, R. J. Noll, R. G. Cooks and Z. Ouyang, in *Chapter 2: Ion Traps for Miniature, Multiplexed, and Soft-Landing Technologies*, ed. R. E. March and J. F. J. Todd, CRC Press, Boca Raton, 2010, pp. 169–247.

2 D. T. Snyder, C. J. Pulliam, Z. Ouyang and R. G. Cooks, *Analytical Chemistry*, 2016, **88**, 2–29.

3 Q. Song, S. Kothari, M. A. Senko, J. C. Schwartz, J. W. Amy, G. C. Stafford, R. G. Cooks and Z. Ouyang, *Analytical Chemistry*, 2006, **78**, 718–725.

4 A. R. Blackler, A. A. Klammer, M. J. MacCoss and C. C. Wu, *Analytical Chemistry*, 2006, **78**, 1337–1344.

5 C. Zhang, H. Chen, A. J. Guymon, G. Wu, R. G. Cooks and Z. Ouyang, *International Journal of Mass Spectrometry*, 2006, **255-256**, 1–10.

6 D. T. Snyder, W.-P. Peng and R. G. Cooks, *Chemical Physics Letters*, 2017, **668**, 69–89.

7 Q. Song, W. Xu, S. A. Smith, L. Gao, W. J. Chappell, R. G. Cooks and Z. Ouyang, *Journal of Mass Spectrometry*, 2010, **45**, 26–34.

8 A. D. Appelhans and D. A. Dahl, *International Journal of Mass Spectrometry*, 2002, **216**, 269–284.

9 R. E. March and R. J. Hughes, *Quadrupole storage mass spectrometry*, John Wiley & Sons, New York, 1989, pp. –.

10 P. M. Remes and G. L. Glish, in *Chapter 17: Collisional Cooling in the Quadrupole Ion Trap Mass Spectrometer (QITMS)*, ed. R. E. March and J. F. J. Todd, CRC Press, Boca Raton, 2010, pp. 739–767.

11 T.-C. Chen, W. Xu and Z. Ouyang, *Rapid Communications in Mass Spectrometry*, 2011, **25**, 3274–3280.

12 B. Brkic, S. Giannoukos, N. France, A. Janulyte, Y. Zerega and S. Taylor, *International Journal of Mass Spectrometry*, 2013, **353**, 36–41.

13 B. Brkic, S. Giannoukos, N. France, R. Murcott, F. Siviero and S. Taylor, *International Journal of Mass Spectrometry*, 2014, **369**, 30–35.

14 A. Janulyte, Y. Zerega, J. Andre, B. Brkic and S. Taylor, *Rapid Communications in Mass Spectrometry*, 2016, **30**, 2407–2415.

15 M. He, D. Guo, Y. Chen, X. Xiong, X. Fang and W. Xu, *Analyst*, 2014, **139**, 6144–6153.

16 M. He, D. Guo, Y. Feng, X. Xiong, H. Zhang, X. Fang and W. Xu, *Journal of Mass Spectrometry*, 2015, **50**, 95–102.

17 S. Schwarz, in *Simulations for Ion Traps Buffer Gas Cooling*, ed. F. Herfurth and H. K. Blaum, Springer Berlin Heidelberg, 2008, vol. 749, pp. 1–21.

18 F. H. Read and N. J. Bowring, *Nuclear Instruments and Methods in Physics Research Section A: Accelerators, Spectrometers, Detectors and Associated Equipment*, 2011, **645**, 273–277.

19 J.-L. Delcroix, *Introduction to the Theory of Ionized Gases*, Interscience Publishers, Paris, 1960.

20 G. Werth, in *Principles of Ion Traps*, ed. F. Herfurth and H. K. Blaum, Springer Berlin Heidelberg, 2008, vol. 749, pp. 1–37.

21 F. Herfurth, J. Dilling, A. Kellerbauer, G. Bollen, S. Henry, H. J. Kluge, E. Lamour, D. Lunney, R. B. Moore, C. Scheidenberger, S. Schwarz, G. Sikler and J. Szerypo, *Nuclear Instruments and Methods in Physics Research Section A: Accelerators, Spectrometers, Detectors and Associated Equipment*, 2001, **469**, 254–275.

22 M. Baril, R. Le and P. Marchand, *International Journal of Mass Spectrometry and Ion Physics*, 1990, **98**, 87–97.

23 A. Drakoudis, M. Söllner and G. Werth, *International Journal of Mass Spectrometry*, 2006, **252**, 61–68.

24 M. Drewsen and A. Bröner, *Physical Review A*, 2000, **62**, 045401–4.

25 C.-H. Chen, T.-C. Chen, X. Zhou, R. Kline-Schoder, P. Sorensen, R. G. Cooks and Z. Ouyang, *Journal of The American Society for Mass Spectrometry*, 2015, **26**, 240–247.

This journal is © The Royal Society of Chemistry [year]